Monthly Notices
of the
ROYAL ASTRONOMICAL SOCIETY

Mon. Not. R. Astron. Soc. **405,** 1444–1457 (2010) doi:10.1111/j.1365-2966.2010.16549.x

# Non-axisymmetric low-frequency oscillations of rotating and magnetized neutron stars

Umin Lee★

*Astronomical Institute, Tohoku University, Sendai, Miyagi 980-8578, Japan*

Accepted 2010 February 18. Received 2010 January 18; in original form 2009 November 16

**ABSTRACT**

We investigate non-axisymmetric low-frequency modes of a rotating and magnetized neutron star, assuming that the star is threaded by a dipole magnetic field whose strength at the stellar surface, $B_0$, is less than $\sim 10^{12}$ G, and whose magnetic axis is aligned with the rotation axis. For modal analysis, we use a neutron star model composed of a fluid ocean, a solid crust and a fluid core, where we treat the core as being non-magnetic assuming that the magnetic pressure is much smaller than the gas pressure in the core. For non-axisymmetric modes, spheroidal modes and toroidal modes are coupled in the presence of a magnetic field even for a non-rotating star. Here, we are interested in low-frequency modes of a rotating and magnetized neutron star whose oscillation frequencies are similar to those of toroidal crust modes of low spherical harmonic degree and low radial order. For a magnetic field of $B_0 \sim 10^7$ G, we find Alfvén waves in the ocean have similar frequencies to the toroidal crust modes, and we find no r modes confined in the ocean for this strength of the field. We calculate the toroidal crustal modes, the interfacial modes peaking at the crust/core interface and the core inertial modes and r modes, and all these modes are found to be insensitive to the magnetic field of strength $B_0 \lesssim 10^{12}$ G. We find the displacement vector of the core $l' = |m|$ r modes have large amplitudes around the rotation axis at the stellar surface even in the presence of a surface magnetic field $B_0 \sim 10^{10}$ G, where $l'$ and $m$ are the spherical harmonic degree and the azimuthal wavenumber of the r modes, respectively. We suggest that millisecond X-ray variations of accretion-powered X-ray millisecond pulsars can be used as a probe into the core r modes destabilized by gravitational wave radiation. If the $l' = |m| = 2$ r mode is excited, we will have the pulsation of the frequency $\sim 4\Omega/3$ with $\Omega$ being the spin frequency of the star.

**Key words:** stars: magnetic fields – stars: neutron – stars: oscillations.

## 1 INTRODUCTION

Oscillation of strongly magnetized neutron stars has attracted an intense attention in recent years, particularly motivated by the discovery of quasi-periodic oscillations (QPOs) of magnetar candidates (e.g. Woods & Thompson 2006), which are believed to be one of the observational manifestations of global oscillations of neutron stars that have a strong global magnetic field of the order of $B_0 \sim 10^{15}$ G at the stellar surface (e.g. Duncan 1998; Israel et al. 2005; Strohmayer & Watts 2005, 2006; Watts & Strohmayer 2006). Thus, recent theoretical studies of the oscillations of magnetized neutron stars have been mainly concerned with the stars having extremely strong surface magnetic fields $B_0 \gtrsim 10^{15}$ G, and these studies have suggested that the QPOs observed in the magnetar candidates are attributable to the toroidal crust modes and Alfvén modes of the neutron stars (e.g. Piro 2005; Glampedakis, Samuelsson & Andersson 2006; Lee 2007, 2008; Sotani, Kokkotas & Stergioulas 2008; Bastrukov et al. 2009; Cerdá-Durán, Stergioulas & Font 2009; Colaiuda, Beyer & Kokkotas 2009; Sotani & Kokkotas 2009). For toroidal modes of strongly magnetized neutron stars, however, it is intriguing, from the theoretical point of view, that Lee (2008) obtained discrete frequency spectra of the magnetic modes, but Sotani et al. (2008), Cerdá-Durán et al. (2009) and Colaiuda et al. (2009), using a different numerical method from that used by Lee (2008), suggested the existence of continuum-frequency spectra of the modes, as originally discussed by Levin (2006, 2007).

The burst oscillation observed in low-mass X-ray binaries (LMXBs) can be another example in which a magnetic field plays an important role in the oscillations of neutron stars, although the strength of the field at the surface of the neutron stars in LMXBs is thought to be less

★E-mail: lee@astr.tohoku.ac.jp

than $\sim 10^{10}$ G, much weaker than that for the magnetar candidates. For the burst oscillation, the hotspot model (e.g. Strohmayer et al. 1997; Cumming & Bildsten 2000; Cumming et al. 2002) and the Rossby wave model (Heyl 2004; Lee 2004) have been proposed, but it seems none of the models is accepted as the one that fully explains the observational properties of the burst oscillation. In the Rossby wave model, Heyl (2004, 2005), Lee (2004) and Lee & Strohmayer (2005) have examined the possibility that the burst oscillation is produced by low-frequency Rossby waves, called r modes in the astrophysical literature, propagating in the surface fluid region (ocean), disregarding the effects of a magnetic field on the low-frequency waves. We note that Bildsten & Cutler (1995) discussed the modal properties of g modes propagating in the fluid ocean above the solid crust of mass-accreting neutron stars as a possible mechanism responsible for the ∼6 Hz QPOs observed in LMXBs. In their paper, on the assumption that the magnetic pressure, $p_B$, is much smaller than the gas pressure, $p$, the critical strength of a magnetic field, $B_c$, below which the magnetic field has no significant effects on the g modes, was estimated to be $B_c \sim 2 \times 10^{10}$ G for the accreted envelopes composed of carbon (see also Piro & Bildsten 2005). Since their argument is based on a local analysis and on the assumption $p_B \ll p$, we think it useful to carry out a global modal analysis of low-frequency waves propagating in the magnetized fluid ocean of a neutron star.

Accretion-powered millisecond X-ray pulsars in LMXBs show small-amplitude, almost sinusoidal X-ray time variations, the dominant period of which is thought to be the spin period of the underlying neutron stars. Lamb et al. (2009) argued that the millisecond X-ray variations are produced by an X-ray-emitting hotspot located at a magnetic pole rotating with the star, and that so long as the symmetry centre of the hotspot is only slightly off the rotation axis the X-ray variations produced have small amplitudes and become almost sinusoidal. They also suggested that if the hotspot is located close to the rotation axis, a slight drift of the hotspot away from the rotation axis leads to appreciable changes in the amplitudes and phases of the X-ray variations. Lamb et al. (2009) pointed out that a temporal change in mass-accretion rates and hence the radius of the magnetosphere, for example, can cause such a drift of the hotspot. We think it is also interesting to consider the possibility that global oscillations of the neutron stars work as a mechanism that perturbs the hotspot periodically.

In this paper, to calculate global oscillations of a rotating and magnetized neutron star, we use the method of series expansion, in which the angular dependence of the perturbations is represented by series expansion in terms of spherical harmonic functions with different spherical harmonic degrees $l$ for a given azimuthal wavenumber $m$ (e.g. Lee & Strohmayer 1996; Lee 2007). We calculate low-$m$, low-frequency modes of a neutron star composed of a fluid ocean, a solid crust and a fluid core, where the star is assumed to be threaded by a dipole magnetic field, the strength $B_0$ of which at the surface is smaller than $\sim 10^{12}$ G. The method of calculation we employ is presented in Section 2, and the numerical results are described in Section 3, and we discuss a local analysis for low-frequency modes in the magnetized fluid ocean in Section 4, and we give discussion and conclusion in Section 5.

## 2 METHOD OF CALCULATION

We consider small-amplitude oscillations of rotating and magnetized neutron stars in Newtonian dynamics, and no general relativistic effects on the oscillations are considered. We employ spherical polar coordinates $(r, \theta, \phi)$, whose origin is at the centre of the star and the axis of rotation is given by $\theta = 0$. We assume a dipole magnetic field given by

$$\boldsymbol{B} = \mu_{\rm m} \nabla(\cos\theta / r^2), \tag{1}$$

where $\mu_{\rm m}$ is the magnetic dipole moment. For simplicity, we also assume that the magnetic axis coincides with the rotation axis. Since the dipole field is a force-free field such that $(\nabla \times \boldsymbol{B}) \times \boldsymbol{B} = 0$, the field does not influence the equilibrium structure of the star. When we assume the axis of rotation is also the magnetic axis, the temporal and azimuthal angular dependence of perturbation can be represented by a single factor $\mathrm{e}^{\mathrm{i}(m\phi+\omega t)}$, where $m$ is the azimuthal wavenumber around the rotation axis and $\omega \equiv \sigma + m\Omega$ is the oscillation frequency observed in the corotating frame of the star, where $\sigma$ is the oscillation frequency in an inertial frame and $\Omega$ is the angular frequency of rotation. The linearized basic equations used in a solid region of the star are given by

$$-\omega^2 \boldsymbol{\xi} + 2\mathrm{i}\omega \boldsymbol{\Omega} \times \boldsymbol{\xi} = \frac{1}{\rho} \nabla \cdot \boldsymbol{\sigma}' - \frac{\rho'}{\rho^2} \nabla \cdot \boldsymbol{\sigma} + \frac{1}{4\pi\rho} \left( \nabla \times \boldsymbol{B}' \right) \times \boldsymbol{B}, \tag{2}$$

$$\rho' + \nabla \cdot (\rho \boldsymbol{\xi}) = 0, \tag{3}$$

$$\frac{\rho'}{\rho} = \frac{1}{\Gamma_1} \frac{p'}{p} - \xi_r A, \tag{4}$$

$$\boldsymbol{B}' = \nabla \times (\boldsymbol{\xi} \times \boldsymbol{B}), \tag{5}$$

where $\rho$ is the mass density, $p$ is the pressure, $\boldsymbol{\xi}$ is the displacement vector, and $\rho'$, $p'$ and $\boldsymbol{B}'$ are the Euler perturbations of the density, the pressure and the magnetic field, respectively, and $A$ is the Schwartzshild discriminant defined by

$$A = \frac{\mathrm{d}\ln\rho}{\mathrm{d}r} - \frac{1}{\Gamma_1} \frac{\mathrm{d}\ln p}{\mathrm{d}r} \tag{6}$$

and

$$\Gamma_1 = \left( \frac{\partial \ln p}{\partial \ln \rho} \right)_{ad}. \tag{7}$$

In equation (2), $\boldsymbol{\sigma}'$ denotes the Eulerian perturbation of the stress tensor, which is derived by using the Lagrangian perturbation of the stress tensor defined, in Cartesian coordinates, by

$$\delta\sigma_{ij} = (\Gamma_1 pu)\,\delta_{ij} + 2\mu\left(u_{ij} - \frac{1}{3}u\delta_{ij}\right), \tag{8}$$

where $u_{ij}$ is the strain tensor given by

$$u_{ij} = \frac{1}{2}\left(\frac{\partial\xi_i}{\partial x_j} + \frac{\partial\xi_j}{\partial x_i}\right), \tag{9}$$

$\mu$ is the shear modulus, $u = \Sigma_{l=1}^{3} u_{ll}$ and $\delta_{ij}$ is the Kronecker delta. Note that we have employed the Cowling approximation neglecting the Eulerian perturbation of the gravitational potential, and that no effects of rotational deformation are included.

We can obtain the equation of motion for a fluid region by replacing the terms $\boldsymbol{\sigma}$ and $\boldsymbol{\sigma}'$ in equation (2) by $-p\delta_{ij}$ and $-p'\delta_{ij}$, respectively, and we do not need to consider equations (8) and (9) for fluid regions.

Since the angular dependence of perturbations in a rotating and magnetized star cannot be represented by a single spherical harmonic function, we expand the perturbed quantities in terms of spherical harmonic functions $Y_l^m(\theta,\phi)$ with different $l$ values for a given $m$, assuming that the axis of rotation coincides with that of the magnetic field. The displacement vector $\boldsymbol{\xi}$ and the perturbed magnetic field $\boldsymbol{B}'$ are then represented by a finite series expansion of length $j_{\max}$ as

$$\frac{\boldsymbol{\xi}}{r} = \sum_{j=1}^{j_{\max}}\left[S_{l_j}(r)Y_{l_j}^m(\theta,\phi)\boldsymbol{e}_r + H_{l_j}(r)\nabla_{\rm H}Y_{l_j}^m(\theta,\phi) + T_{l'_j}(r)\boldsymbol{e}_r\times\nabla_{\rm H}Y_{l'_j}^m(\theta,\phi)\right]{\rm e}^{{\rm i}\omega t} \tag{10}$$

and

$$\frac{\boldsymbol{B}'}{B_0(r)} = \sum_{j=1}^{j_{\max}}\left[b_{l'_j}^{\rm S}(r)Y_{l'_j}^m(\theta,\phi)\boldsymbol{e}_r + b_{l'_j}^{\rm H}(r)\nabla_{\rm H}Y_{l'_j}^m(\theta,\phi) + b_{l_j}^{\rm T}(r)\boldsymbol{e}_r\times\nabla_{\rm H}Y_{l_j}^m(\theta,\phi)\right]{\rm e}^{{\rm i}\omega t}, \tag{11}$$

and the pressure perturbation, $p'$, for example, is given by

$$p' = \sum_{j=1}^{j_{\max}} p'_{l_j}(r)Y_{l_j}^m(\theta,\phi){\rm e}^{{\rm i}\omega t}, \tag{12}$$

where

$$\nabla_{\rm H} = \boldsymbol{e}_\theta\frac{\partial}{\partial\theta} + \boldsymbol{e}_\phi\frac{1}{\sin\theta}\frac{\partial}{\partial\phi} \tag{13}$$

and $B_0(r) = \mu_{\rm m}/r^3$, and $l_j = |m| + 2(j-1)$ and $l'_j = l_j + 1$ for even modes, and $l_j = |m| + 2j - 1$ and $l'_j = l_j - 1$ for odd modes, respectively, with $j = 1, 2, 3, \ldots, j_{\max}$. Substituting the expansions (10), (11) and (12) into the linearized basic equations (2)–(5) and (8), we obtain a finite set of coupled linear ordinary differential equations for the expansion coefficients $S_{l_j}$, $H_{l_j}$, $T_{l'_j}$ and so on, which we call the oscillation equation. For non-axisymmetric modes with $m \neq 0$, we cannot expect decoupling between spheroidal (polar) modes and toroidal (axial) modes even for $\Omega = 0$, although for axisymmetric modes with $m = 0$, spheroidal modes and toroidal modes are decoupled when $\Omega = 0$ (e.g. Lee 2007).

In this paper, we treat for simplicity the fluid core being non-magnetic, which may be justified if we assume the magnetic pressure is much smaller than the gas pressure in the core. This justification, however, could not be fully granted, e.g. for r modes in the core of a sufficiently slowly rotating neutron star since magnetic tension would possibly affect the modes even if the magnetic pressure is smaller than the gas pressure in the core. The oscillation equations used in the magnetized regions are given in Appendix A, in which the jump conditions imposed at the solid/fluid interfaces and the boundary conditions applied at the stellar centre and the surface are also given. The oscillation equation used in the non-magnetic fluid core is found, for example, in the appendix of Lee & Saio (1990).

## 3 NUMERICAL RESULTS

For the neutron star model used for modal analysis, we employ a cooling evolution model called NS05T7, which was calculated by Richardson et al. (1982). The mass of the model is $M \sim 0.5\,{\rm M}_\odot$ and the central temperature is $T \sim 10^7$ K, and the model is composed of a fluid ocean, a solid crust and a fluid core, and because of density stratification g modes propagate in the fluid regions. The more detailed properties of the model, such as the equations of state used, are described, for example, by McDermott, Van Horn & Hansen (1988), who carried out modal analysis of the model assuming no rotation and no magnetic fields. Since this is a low-mass model, the solid crust is rather thick, and the low radial order crustal modes of low spherical harmonic degree $l$ are well separated from the $f$ and $p$ modes of the model, which makes the modal analysis much simpler than the case in which the crustal modes have frequencies similar to those of the f and p modes as expected for more massive neutron stars with accreted envelopes.

Let us begin with the case of a weak magnetic field of strength $B_0 = 10^7$ G. In the presence of a magnetic field, the existence of Alfvén waves, whose oscillation frequency depends on the strength of the magnetic field and on the direction of wave propagation relative to the magnetic field, inevitably makes frequency spectra complex. For the case of $B_0 = 10^7$ G, the frequency spectra of low-frequency modes are too complicated to calculate completely, as suggested by Fig. 1, which plots the oscillation frequency $\omega$ of low-frequency $|m| = 1$ modes as functions of $\Omega$ for even modes (left-hand panel) and odd modes (right-hand panel), respectively, where we have used $j_{\max} = 10$. We note

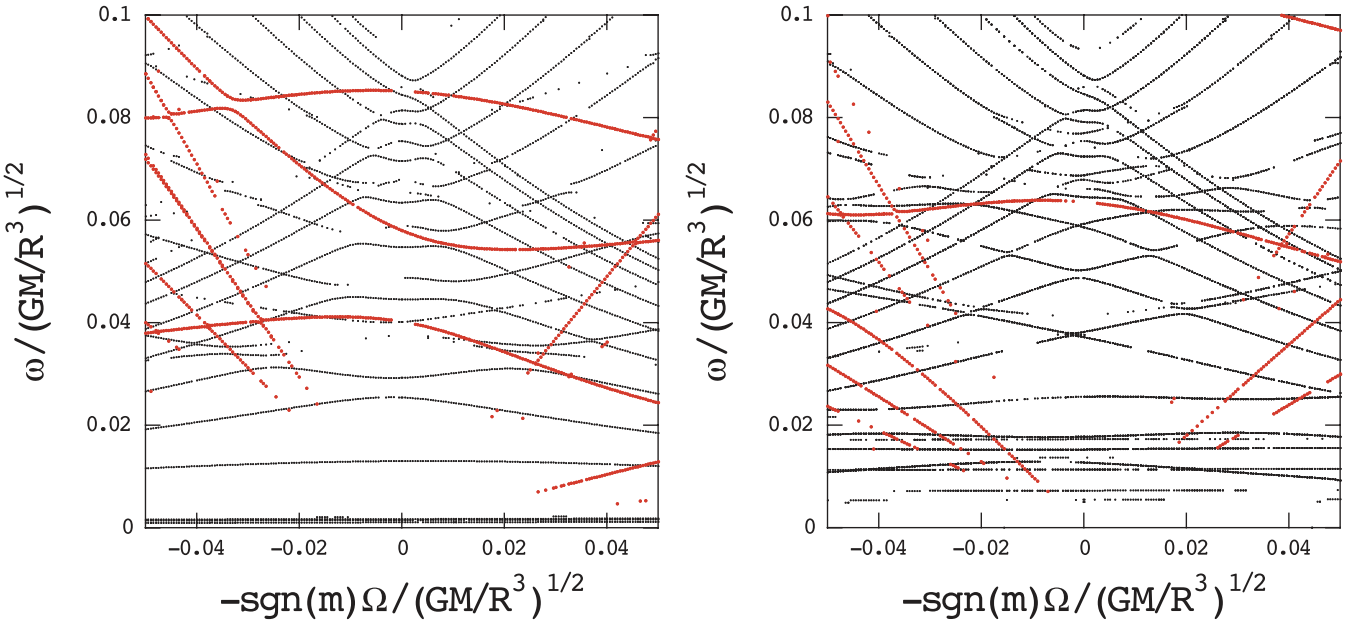


**Figure 1.** Low-frequency $|m| = 1$ modes of the model NS05T7 are plotted as functions of $-\mathrm{sgn}(m)\Omega$ for the case of $B_0 = 10^7$ G for even modes in the left-hand panel and odd modes in the right-hand panel, where $\mathrm{sgn}(m) = m/|m|$ and the positive and negative sides of the horizontal axis are for prograde and retorgrade modes, respectively. The black dots and red dots represent the ocean modes and core/crust modes, respectively.

that there appear in Fig. 1 several kinds of modes, that is, the inertial modes and r modes in the fluid core, the toroidal crust modes, the interfacial modes whose $\xi_r$ amplitudes peak at the interface between the core and the solid crust, and the modes confined in the fluid ocean. The inertial modes and r modes are rationally induced modes, whose oscillation frequencies are approximately proportional to $\Omega$ and are found on almost straight lines tending to the origin in the figure, where the r modes appear on the side of retrograde modes. The loci of the oscillation frequencies $\omega$ as functions of $\Omega$ for the core inertial modes, r modes, the toroidal crust modes and the interfacial modes are more clearly seen for the case of a stronger magnetic field of $B_0 = 10^{10}$ G as shown in Fig. 2 below. We note that the toroidal crust modes are insensitive to the magnetic field of strength $B_0 \lesssim 10^{12}$ (e.g. Lee 2007), and that the inertial modes and r modes in the fluid core and the interfacial mode at the core/crust interface are not strongly affected by the magnetic field even if their eigenfunctions extend to the surface through the magnetized solid crust and fluid ocean.

However, the modes that are confined in the surface ocean are strongly influenced by a magnetic field as weak as $B_0 \sim 10^7$ G and show extremely complicated frequency spectra. Although there usually appear gravito-inertial modes and r modes as non-axisymmetric low-frequency modes confined in the ocean for a non-magnetized neutron star, we find no ocean r modes in the presence of a magnetic field, even if it is as weak as $B_0 \sim 10^7$ G. We also find that Alfvén modes come into the frequency spectra of the low-frequency modes, modifying the spectra of the gravito-inertial modes. We note that there exist two branches of modes in Fig. 1. In one branch of modes, the oscillation frequency $\omega$ increases as $|\Omega|$ increases, while the oscillation frequency decreases with increasing $|\Omega|$ in the other, although there occurs frequent avoided crossings between the two branches of modes as $\Omega$ varies. Based on the local analysis presented in Section 4, we think the former can be regarded as (gravito-)inertial modes and the latter as Alfvén modes. However, we have to note that the eigenfrequencies of the modes in the two branches do not necessarily reach good convergence even if $j_{\max}$ is increased to $j_{\max} \sim 20$. In this sense we are not sure that the modes confined in the surface ocean we calculate are discrete modes with real frequencies.

In Fig. 2, we plot low-frequency $|m| = 1$ modes against $\Omega$ for the case of $B_0 = 10^{10}$ G for even modes (left-hand panel) and odd modes (right-hand panel), where we have used $j_{\max} = 10$. In the figure, the symbols ${}_{l'}t_n$, ${}_{l}i_2$ and ${}_{l'}r_n$, respectively, denote the toroidal crust modes, the interfacial mode whose $\xi_r$ amplitudes peak at the core/crust interface and the core r modes whose frequency $\omega$ tends to $2m\Omega/\left[l'(l'+1)\right]$ as $\Omega \to 0$, where $l$ and $l'$ denote the spherical harmonic degrees and the subscript $n$ indicates the radial order, usually corresponding to the number of nodes of the dominant eigenfunction in the propagation region. Note that we do not attach any labels to inertial modes in the fluid core whose frequencies are approximately proportional to $\Omega$ and are found on almost straight lines tending to the origin of the figure. Because the fluid core is almost isentropic such that the Brunt–Väisälä frequency $N$ is extremely small, the odd r mode labelled ${}_{l'=|m|}r_{n=0}$ is the only r mode we can find for a given value of $m$ (e.g. Yoshida & Lee 2000a). We note that the eigenfrequencies of the modes plotted in Fig. 2 obtain good convergence when $j_{\max}$ is increased to $j_{\max} \gtrsim 10$. We have calculated low-frequency $|m| = 1$ modes for $B_0 = 10^{12}$ G in the same frequency range as that in Fig. 2, and obtained the result quite similar to that for the case of $B_0 = 10^{10}$ G.

Because of the effects of rotation, the frequencies $\omega$ of the toroidal crust modes and the interfacial mode vary as $\Omega$ changes. If we expand the oscillation frequency of a mode as $\omega = \omega_0 + mC_1\Omega + O(\Omega^2)$, where $\omega_0$ is the frequency of the mode for $\Omega = 0$, the $C_1$ coefficient describes the first-order response of the oscillation frequency to small $\Omega$, and a list of the $C_1$ coefficients of $m = 2$ spheroidal modes of the model NS05T7 is tabulated in Lee & Strohmayer (1996), where no magnetic effects are considered. For the toroidal crustal modes, on the

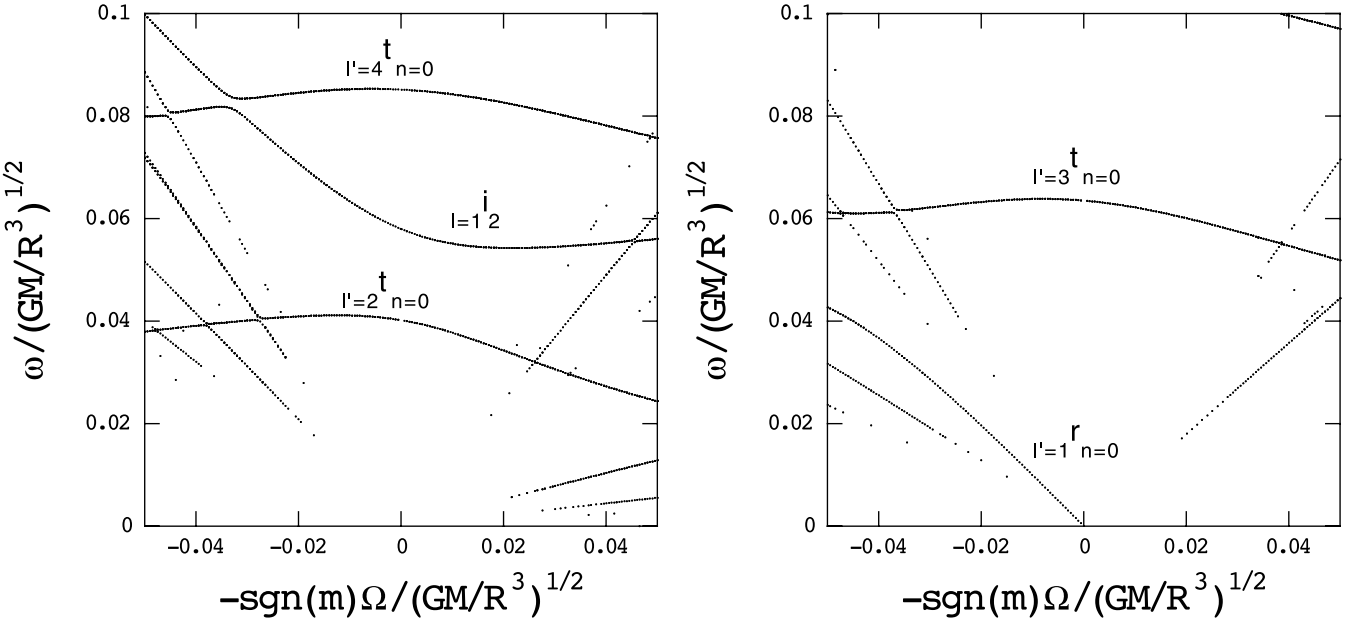


**Figure 2.** Low-frequency $|m| = 1$ modes of the model NS05T7 plotted versus $-\mathrm{sgn}(m)\Omega$ for the case of $B_0 = 10^{10}$ G for even modes in the left-hand panel and odd modes in the right-hand panel, where sgn(m) $= m/|m|$ and the negative and positive sides of the horizontal axis are for retrograde and prograde modes, respectively. The symbols ${}_{l'}t_n$, ${}_{l}i_2$ and ${}_{l'}r_n$ denote the toroidal crust modes, the interfacial mode whose amplitudes peak at the core/crust interface, and the core r mode, respectively, where $l$ and $l'$ denote the spherical harmonic degrees and the subscript $n$ is the radial order, which is usually equal to the number of radial nodes of the dominant component of the eigenfunctions.

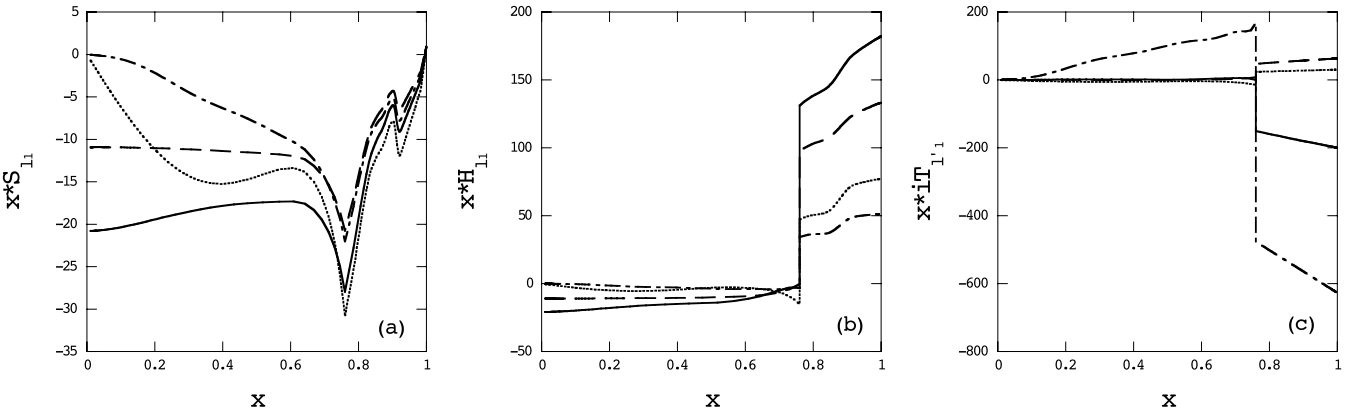


**Figure 3.** Eigenfunctions $xS_{l_1}$ (panel a), $xH_{l_1}$ (panel b) and $xiT_{l'_1}$ (panel c) plotted against $x \equiv r/R$ for the low-frequency $|m| = 1$ modes for the case of $B_0 = 10^{10}$ G and $\Omega/\sqrt{GM/R^3} = 0.04$, where we use $j_{\max} = 10$. In each panel, the solid line is for the even toroidal crustal mode ${}_{l'=2}t_{n=0}$, the dashed line for the even interfacial mode ${}_{l=1}i_2$, the dash–dotted line for the odd r-mode ${}_{l'=1}r_{n=0}$, and the dotted line for the odd toroidal crustal mode ${}_{l'=3}t_{n=0}$. Note that the amplitude normalization is given by $xS_{l_1} = 1$ at the stellar surface. Except for the r mode, which is a retrograde mode with $m = 1$, all the other modes are prograde modes with $m = -1$.

other hand, Lee & Strohmayer (1996) showed $C_1 = 1/\left[l'\left(l'+1\right)\right]$ for non-magnetized stars. Note that for rotationally induced modes such as inertial modes and r modes, we have $\omega_0 = 0$. Fig. 2 indicates that the frequency behaviour of the crust modes for slow rotation is consistent to that expected from the $C_1$ coefficients, even in the presence of a magnetic field of strength $B_0 \sim 10^{10}$ G, although it is also clear that as $|\Omega|$ increases from $\Omega = 0$, the deviation of $\omega$ from the expansion $\omega_0 + mC_1\Omega$ quickly becomes significant. The deviation of the frequency from the expansion may be partly caused by avoided crossings between two different modes. An example found in Fig. 2 is the avoided crossing between ${}_{l'=2}t_{n=0}$ and ${}_{l=1}i_2$, which is a crossing between a toroidal mode and a spheroidal mode.

In Fig. 3, we plot the eigenfunctions $xS_{l_1}(x)$, $xH_{l_1}(x)$ and $xiT_{l'_1}(x)$ of several low-frequency $|m| = 1$ modes for the case of $B_0 = 10^{10}$ G and $\Omega/\sqrt{GM/R^3} = 0.04$, where $x \equiv r/R$, and the low-frequency modes we plot are the even toroidal crust mode ${}_{l'=2}t_{n=0}$, the even interfacial mode ${}_{l=1}i_2$, the odd r-mode ${}_{l'=1}r_{n=0}$ and the odd toroidal crustal mode ${}_{l'=3}t_{n=0}$, and except for the r mode, which is a retrograde mode with $m = 1$, all the other modes are prograde modes with $m = -1$. Note that the toroidal crustal modes have appreciable amplitudes in the fluid core due to the effects of rotation. We find the eigenfunctions of the modes in the presence of the dipole magnetic field of $B_0 = 10^{10}$ G are quite similar to those found in the absence of the magnetic field (see e.g. Lee & Strohmayer 1996; Yoshida & Lee 2001), suggesting that these modes are not strongly affected by magnetic fields of that strength. Note that in the vicinity of the stellar centre, since the eigenfunctions

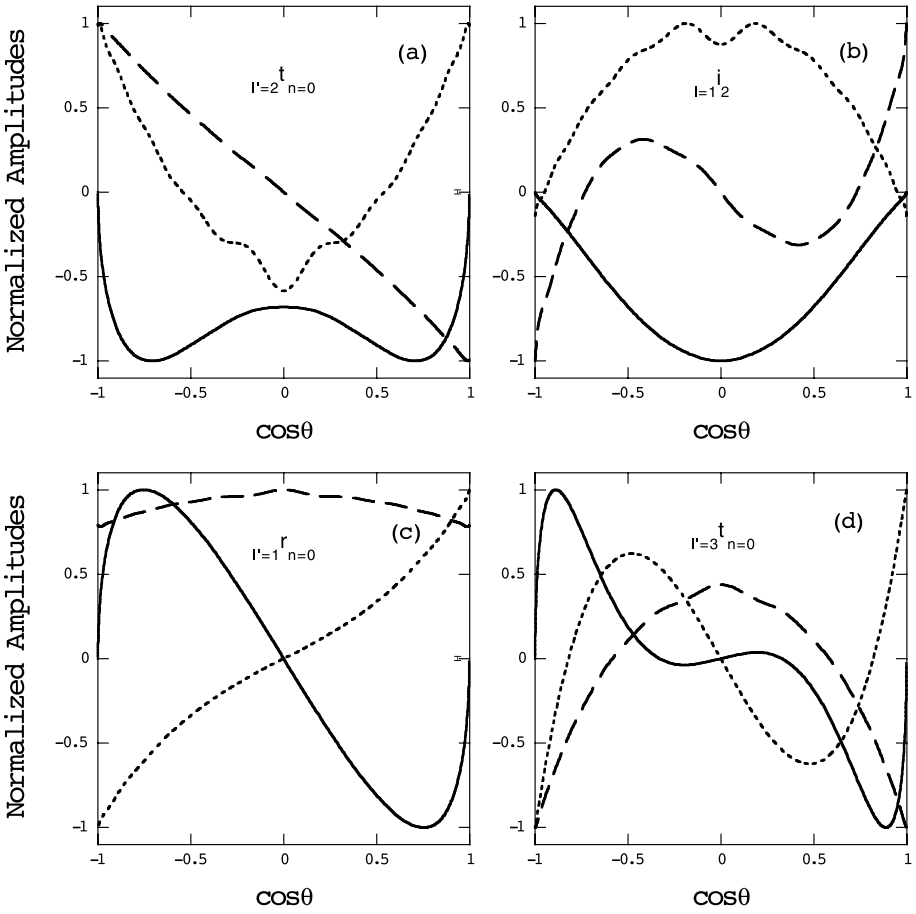


**Figure 4.** Functions $X^r(\theta)$, $X^\theta(\theta)$ and $X^\phi(\theta)$ versus $\cos\theta$ for the low-frequency $|m| = 1$ modes for the case of $B_0 = 10^{10}$ G and $\Omega/\sqrt{GM/R^3} = 0.04$ for $j_{\max} = 10$, where the functions are evaluated at the stellar surface, and the solid, dashed and dotted lines denote the functions $X^r(\theta)$, $X^\theta(\theta)$ and $X^\phi(\theta)$, respectively. Panels (a), (b), (c) and (d) are for the even toroidal crust mode ${}_{l'=2}t_{n=0}$, the even interfacial mode ${}_{l=1}i_2$, the odd core ${}_{l'=1}r_{n=0}$ mode, and the odd toroidal crust mode ${}_{l'=3}t_{n=0}$, respectively, where only the r mode is a retrograde mode with $m = 1$, and the others are prograde modes with $m = -1$. The functions are normalized by their maximum amplitudes. The functions $X^r(\theta)$ and $X^\phi(\theta)$ of even (odd) modes are symmetric (antisymmetric) with respect to the axis of $\cos\theta = 0$, while the function $X^\theta(\theta)$ of even (odd) modes is antisymmetric (symmetric).

$S_{l_1}$ and $H_{l_1}$ are approximately proportional to $x^{l_1-2}$ (e.g. Unno et al. 1989), the functions $xS_{l_1}$ and $xH_{l_1}$ behave as $\propto x^0$ for even modes of $l_1 = |m| = 1$ and as $\propto x^1$ for odd modes of $l_1 = |m| + 1 = 2$, as indicated by panels (a) and (b).

From the observational point of view, it is useful to know the $\theta$ dependence of the displacement vector of the modes at the surface of the star. As noted in the previous section, for rotating and magnetized stars, the eigenfunction of an oscillation mode cannot be represented by a single spherical harmonic function $Y_l^m(\theta, \phi)$ and hence their surface pattern can be largely different from that for non-magnetic and non-rotating stars. To see the angular dependence of the displacement vector at the surface, we introduce the functions $X^j(\theta)$ defined by

$$X^r(\theta)\,\mathrm{e}^{\mathrm{i}m\phi} = \sum_{j=1}^{j_{\max}} S_{l_j}(R)\,Y_{l_j}^m(\theta,\phi)\,, \tag{14}$$

$$X^\theta(\theta)\,\mathrm{e}^{\mathrm{i}m\phi} = \boldsymbol{e}_\theta \sum_{j=1}^{j_{\max}} \left[H_{l_j}(R)\nabla_{\mathrm{H}}Y_{l_j}^m(\theta,\phi) + T_{l'_j}(R)\boldsymbol{e}_r\nabla_{\mathrm{H}}Y_{l'_j}^m(\theta,\phi)\right], \tag{15}$$

$$X^\phi(\theta)\,\mathrm{e}^{\mathrm{i}m\phi} = -\mathrm{i}\boldsymbol{e}_\phi \sum_{j=1}^{j_{\max}} \left[H_{l_j}(R)\nabla_{\mathrm{H}}Y_{l_j}^m(\theta,\phi) + T_{l'_j}(R)\boldsymbol{e}_r\nabla_{\mathrm{H}}Y_{l'_j}^m(\theta,\phi)\right]. \tag{16}$$

In Fig. 4, we plot the functions $X^j(\theta)$ of the low-frequency modes presented in Fig. 3 for the case of $B_0 = 10^{10}$ G and $\Omega/\sqrt{GM/R^3} = 0.04$, where in each of the panels the solid, dashed and dotted lines in each panel, respectively, denote the functions $X^r$, $X^\theta$ and $X^\phi$, which are normalized by their maximum amplitudes. Since the modes have low frequencies, the maximum amplitudes of $\xi_r$ are much smaller than those of $\xi_\theta$ and $\xi_\phi$, that is, the horizontal and/or toroidal components of the displacement vector are dominant over the radial component. It is to be noted that although the amplitudes of the ocean r modes tend to be confined to the equatorial regions (see e.g. Lee 2004), this is not the case for the $l' = |m|$ r modes in the fluid core, which have large amplitudes in the regions around the poles.

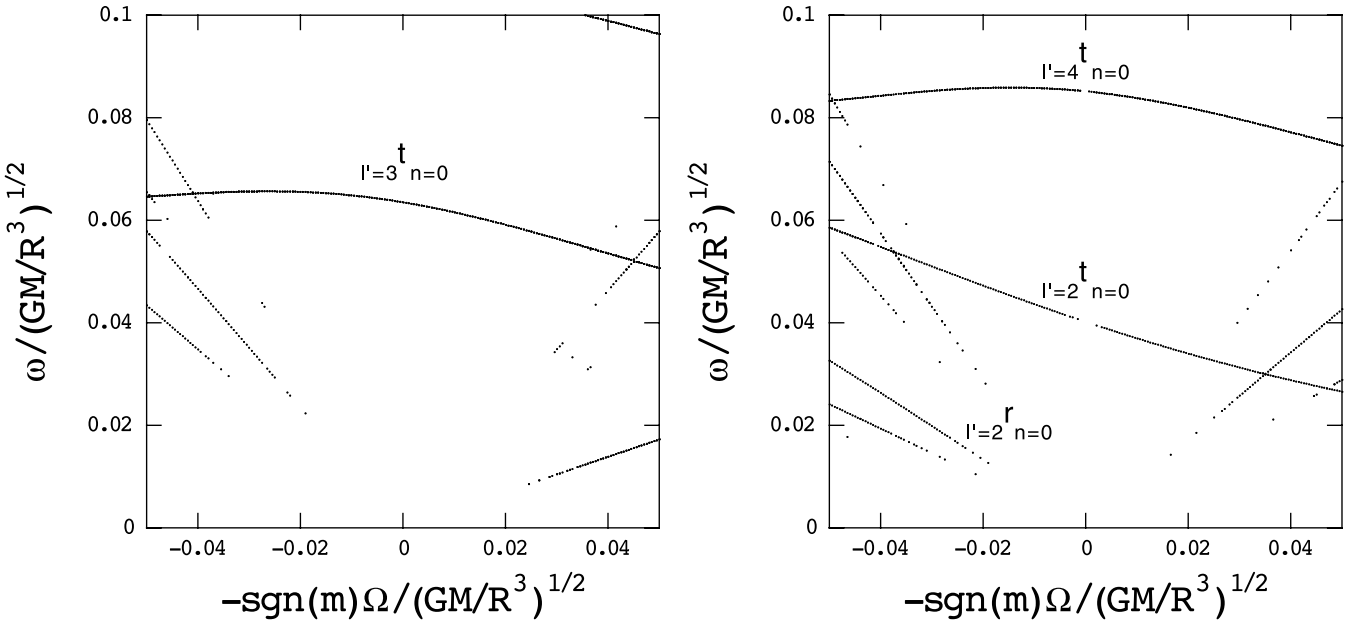


**Figure 5.** Same as Fig. 2 but for $|m| = 2$.

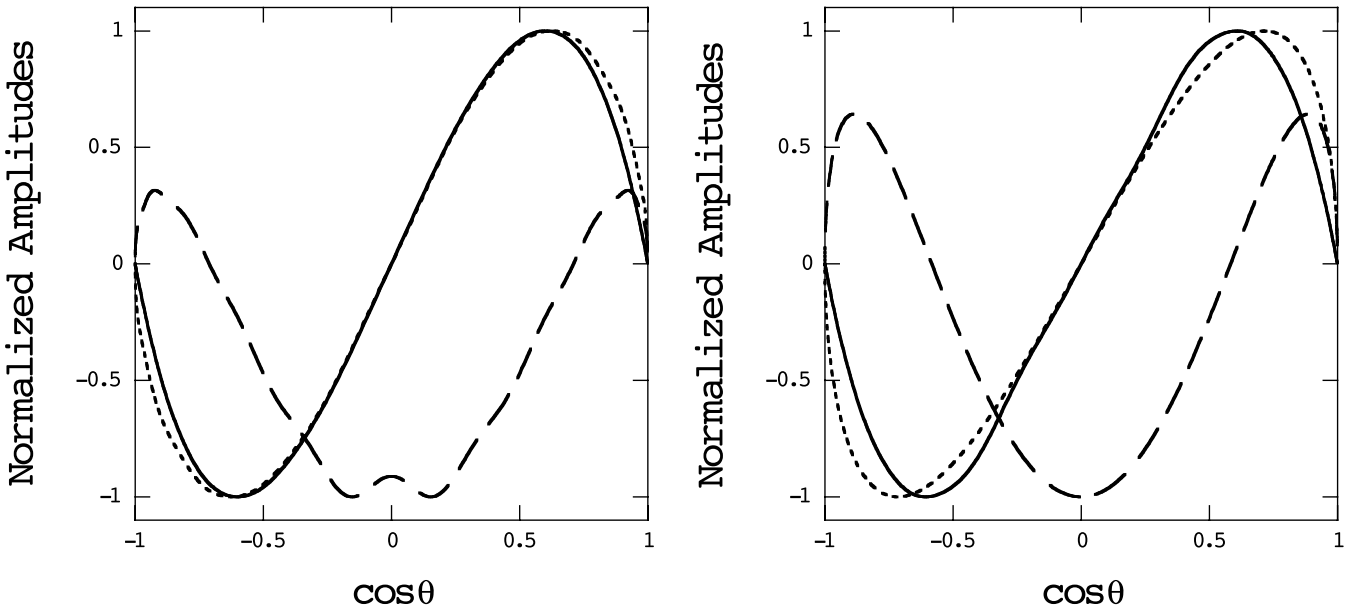


**Figure 6.** Functions $X^r(\theta)$, $X^\theta(\theta)$ and $X^\phi(\theta)$ at the surface versus $\cos\theta$ for the $m = 2\,_{l'=2}r_{n=0}$ mode for the cases of $B_0 = 10^{10}$ G in the left-hand panel and $B_0 = 0$ G in the right-hand panel, where $\Omega/\sqrt{GM/R^3} = 0.04$ and $j_{\max} = 10$ are assumed. The solid, dashed and dotted lines, respectively, denote the functions $X^r(\theta)$, $X^\theta(\theta)$ and $X^\phi(\theta)$, which are normalized by their maximum amplitudes.

In Fig. 5, we plot the frequencies $\omega$ of low-frequency $|m| = 2$ modes against $\Omega$ for the case of $B_0 = 10^{10}$ G for even modes (left-hand panel) and odd modes (right-hand panel), where we have used $j_{\max} = 10$. For the case of $|m| = 2$, the toroidal crustal mode $_{l'=3}t_{n=0}$ appears as an even mode, while $_{l'=2}t_{n=0}$ and $_{l'=4}t_{n=0}$ as an odd mode. We note that no interfacial modes appear in the frequency range shown in the figure. Fig. 6 shows the functions $X^j(\theta)$ versus $\cos\theta$ for the core $l' = m = 2$ r mode at $\Omega/\sqrt{GM/R^3} = 0.04$ for $B_0 = 10^{10}$ G (left-hand panel) and $B_0 = 0$ G (right-hand panel), where the functions, evaluated at the stellar surface, are normalized by their maximum amplitudes. This figure shows that the surface pattern generated by the core $l' = m = 2$ r mode is not affected by the field as strong as $B_0 = 10^{10}$ G, which is also the case for the core $l' = m = 1$ r mode.

## 4 LOCAL ANALYSIS

To gain an understanding of the low-frequency modes confined in the shallow fluid ocean calculated for the case of $B_0 = 10^7$ G, we apply a local analysis to low-frequency modes in a fluid region of a rotating and magnetized neutron star. Note that a local analysis of waves in

rotating stars with no magnetic fields is found in, for example, Unno et al. (1989). In this section, we assume that the $\boldsymbol{x}$ and $t$ dependence of the perturbed quantities is given by the function $\exp[\mathrm{i}(\boldsymbol{k}\cdot\boldsymbol{x}+\omega t)]$, where $\boldsymbol{k}$ is the wavenumber vector. Using the equation of motion for a fluid region and equations (3)–(5), we can derive a set of equations used for the local analysis:

$$-\omega^2\boldsymbol{\xi}+2\mathrm{i}\omega\boldsymbol{\Omega}\times\boldsymbol{\xi}=-\frac{1}{\rho}\mathrm{i}\boldsymbol{k}p'+\frac{\rho'}{\rho^2}\nabla p+\frac{1}{4\pi\rho}\left(\mathrm{i}\boldsymbol{k}\times\boldsymbol{B}'\right)\times\boldsymbol{B}, \tag{17}$$

$$\rho'+\mathrm{i}\rho\left(\boldsymbol{k}\cdot\boldsymbol{\xi}\right)+\boldsymbol{\xi}\cdot\nabla\rho=0, \tag{18}$$

$$p'=\Gamma_1 p\left(\boldsymbol{\xi}\cdot\boldsymbol{A}+\rho'/\rho\right), \tag{19}$$

$$\boldsymbol{B}'=\mathrm{i}\boldsymbol{k}\times\left(\boldsymbol{\xi}\times\boldsymbol{B}\right), \tag{20}$$

which are combined to give

$$\left[\omega^2-\frac{(\boldsymbol{k}\cdot\boldsymbol{B})^2}{4\pi\rho}\right]\boldsymbol{\xi}-\left[\left(a^2+a_{\mathrm{A}}^2\right)\boldsymbol{k}-\frac{(\boldsymbol{k}\cdot\boldsymbol{B})}{4\pi\rho}\boldsymbol{B}\right](\boldsymbol{k}\cdot\boldsymbol{\xi})+\frac{(\boldsymbol{k}\cdot\boldsymbol{B})(\boldsymbol{\xi}\cdot\boldsymbol{B})}{4\pi\rho}\boldsymbol{k}-2\mathrm{i}\omega\boldsymbol{\Omega}\times\boldsymbol{\xi}-\mathrm{i}a^2(\boldsymbol{\xi}\cdot\boldsymbol{A})\boldsymbol{k}-\mathrm{i}(\boldsymbol{k}\cdot\boldsymbol{\xi})\frac{\nabla p}{\rho}=0, \tag{21}$$

where $a=\sqrt{\Gamma_1 p/\rho}$ is the adiabatic sound speed and $a_{\mathrm{A}}=B/\sqrt{4\pi\rho}$ is the Alfvén velocity and $B=|\boldsymbol{B}|$.

To make the local analysis tractable, we employ a local Cartesian coordinate system whose $z$-axis is along the radial direction, and we assume that $\boldsymbol{\Omega}=\Omega_z\boldsymbol{e}_z$ neglecting the local horizontal component of the rotation vector. Equation (21) can be rewritten into a form $\mathbf{W}\boldsymbol{\xi}=0$ with $\mathbf{W}$ being a matrix, and the condition $\det\mathbf{W}=0$ leads to the dispersion relation

$$\omega^6+A_4\omega^4+A_2\omega^2+A_1\omega+A_0=0, \tag{22}$$

where

$$A_4=-\left(a^2+a_{\mathrm{A}}^2\right)k^2-a_{\mathrm{A}}^2k^2\cos^2\theta-(2\Omega_z)^2-\beta^2, \tag{23}$$

$$A_2=\left(2a^2+a_{\mathrm{A}}^2\right)a_{\mathrm{A}}^2k^4\cos^2\theta+a^2k_{\mathrm{H}}^2N^2+(2\Omega_z)^2\left[a^2k_z^2+a_{\mathrm{A}}^2k^2\left(\cos^2\theta+\frac{k_z^2}{k^2}-2\cos\theta\frac{B_z}{B}\frac{k_z}{k}\right)\right]$$
$$+\left[a_{\mathrm{A}}^2k_{\mathrm{H}}^2+2a_{\mathrm{A}}^2k^2\cos\theta\frac{B_z}{B}\frac{k_z}{k}+(2\Omega_z)^2\right]\beta^2, \tag{24}$$

$$A_1=-4a_{\mathrm{A}}^2gk^2k_z\Omega_z\frac{k_{\mathrm{H}}}{k}\frac{B_{\mathrm{H}}}{B}\sin\psi\cos\theta, \tag{25}$$

$$A_0=-a^2a_{\mathrm{A}}^2k^4\cos^2\theta\left(a_{\mathrm{A}}^2k^2\cos^2\theta+\frac{k_{\mathrm{H}}^2}{k^2}N^2\right)-a_{\mathrm{A}}^4k^4\cos^2\theta\frac{B_z^2}{B^2}\beta^2, \tag{26}$$

where $g=GM_r/r^2$, $\cos\theta=(\boldsymbol{k}\cdot\boldsymbol{B})/(kB)$, $k=|\boldsymbol{k}|$, $B_{\mathrm{H}}=\sqrt{B_x^2+B_y^2}$, $k_{\mathrm{H}}=\sqrt{k_x^2+k_y^2}$, $\sin\psi=(\boldsymbol{k}\times\boldsymbol{B})_z/(k_{\mathrm{H}}B_{\mathrm{H}})$, $N=\sqrt{-gA}$ (the Brunt–Väisälä frequency) and

$$\beta^2\equiv-\frac{\mathrm{d}\ln\rho}{\mathrm{d}z}g=N^2+\frac{g^2}{a^2}. \tag{27}$$

Note that the term proportional to $A_1$ breaks the symmetry given by $\omega(-\Omega_z)=\omega(\Omega_z)$.

If we assume $\boldsymbol{B}=0$ and $\boldsymbol{\Omega}\neq0$, the dispersion relation reduces to

$$\omega^2\left\{\omega^4-\left[a^2k^2+(2\Omega_z)^2+\beta^2\right]\omega^2+\left[a^2k_z^2(2\Omega_z)^2+a^2k_{\mathrm{H}}^2N^2+(2\Omega_z)^2\beta^2\right]\right\}=0, \tag{28}$$

the non-trivial solution of which is

$$\omega^2=\frac{1}{2}\left\{a^2k^2+(2\Omega_z)^2+\beta^2\pm\sqrt{\left[a^2k^2+\beta^2-(2\Omega_z)^2\right]^2-4a^2k_{\mathrm{H}}^2\left[N^2-(2\Omega_z)^2\right]}\right\}. \tag{29}$$

On the other hand, if we assume $\boldsymbol{\Omega}=0$ and $\boldsymbol{B}\neq0$, the dispersion relation reduces to

$$\left(\omega^2-a_{\mathrm{A}}^2k^2\cos^2\theta\right)\left[\omega^4-\left(a^2k^2+a_{\mathrm{A}}^2k^2+\beta^2\right)\omega^2+a^2k^2\left(a_{\mathrm{A}}^2k^2\cos^2\theta+\frac{k_{\mathrm{H}}^2}{k^2}N^2\right)+a_{\mathrm{A}}^2k^2\left(\frac{B_z^2}{B^2}+\frac{k_{\mathrm{H}}^2}{k^2}\frac{B_{\mathrm{H}}^2}{B^2}\sin^2\psi\right)\beta^2\right]$$
$$+a_{\mathrm{A}}^4k^4\frac{k_{\mathrm{H}}^2}{k^2}\frac{B_{\mathrm{H}}^2}{B^2}\sin^2\psi\cos^2\theta\beta^2=0. \tag{30}$$

If we can further assume $\sin\psi=0$, the solutions of the dispersion relation are separated into

$$\omega^2=a_{\mathrm{A}}^2k^2\cos^2\theta, \tag{31}$$

corresponding to the Alfvén waves, and to

$$\omega^2=\frac{1}{2}\left\{\left(a^2+a_{\mathrm{A}}^2\right)k^2+\beta^2\pm\sqrt{\left[\left(a^2+a_{\mathrm{A}}^2\right)k^2+\beta^2\right]^2-4a^2k^2\left(a_{\mathrm{A}}^2k^2\cos^2\theta+\frac{k_{\mathrm{H}}^2}{k^2}N^2+\frac{a_{\mathrm{A}}^2}{a^2}\frac{B_z^2}{B^2}\beta^2\right)}\right\}. \tag{32}$$

For the case of $\boldsymbol{B} \neq 0$ and $\boldsymbol{\Omega} \neq 0$, it is difficult to analytically solve the dispersion relation (22) in general. Here, we numerically solve equation (22), which can be rewritten, by normalizing various quantities, as

$$\bar{\omega}^6 + \frac{A_4}{\Omega_0^2}\bar{\omega}^4 + \frac{A_2}{\Omega_0^4}\bar{\omega}^2 + \frac{A_1}{\Omega_0^5}\bar{\omega} + \frac{A_0}{\Omega_0^6} = 0, \tag{33}$$

where

$$\frac{A_4}{\Omega_0^2} = -(p+q)(Rk)^2 - q(Rk)^2\cos^2\theta - 4\bar{\Omega}_z^2 - \frac{\beta^2}{\Omega_0^2}, \tag{34}$$

$$\frac{A_2}{\Omega_0^4} = (2p+q)q(Rk)^4\cos^2\theta + p(Rk)^2\frac{k_{\rm H}^2}{k^2}\bar{N}^2 + 4\bar{\Omega}_z^2\left[p(Rk)^2\frac{k_z^2}{k^2} + q(Rk)^2\left(\cos^2\theta + \frac{k_z^2}{k^2} - 2\cos\theta\frac{B_z}{B}\frac{k_z}{k}\right)\right] + \left[q(Rk)^2\frac{k_{\rm H}^2}{k^2} + 2q(Rk)^2\cos\theta\frac{B_z}{B}\frac{k_z}{k} + 4\bar{\Omega}_z^2\right]\frac{\beta^2}{\Omega_0^2}, \tag{35}$$

$$\frac{A_1}{\Omega_0^5} = -4q\frac{g}{g_S}(Rk)^3\,\bar{\Omega}_z\frac{k_z}{k}\frac{k_{\rm H}}{k}\frac{B_{\rm H}}{B}\sin\psi\cos\theta, \tag{36}$$

$$\frac{A_0}{\Omega_0^6} = -pq(Rk)^4\cos^2\theta\left[q(Rk)^2\cos^2\theta + \frac{k_{\rm H}^2}{k^2}\bar{N}^2\right] - q^2(Rk)^4\cos^2\theta\frac{B_z^2}{B^2}\frac{\beta^2}{\Omega_0^2}, \tag{37}$$

where

$$p = \frac{a^2}{(R\Omega_0)^2}, \quad q = \frac{a_{\rm A}^2}{(R\Omega_0)^2}, \quad \bar{N}^2 = \frac{N^2}{\Omega_0^2}, \quad g_S = \frac{GM}{R^2}, \quad \bar{\Omega}_z = \frac{\Omega_z}{\Omega_0}, \quad \bar{\omega} = \frac{\omega}{\Omega_0}, \quad \Omega_0 = \sqrt{\frac{GM}{R^3}}. \tag{38}$$

To solve the dispersion relation for a given neutron star model with $M$ and $R$ and for a given magnetic field $\boldsymbol{B}$, we need to supply with appropriate values the following parameters:

$$p, \quad q, \quad \bar{N}^2, \quad \bar{\Omega}_z, \quad (Rk), \quad \cos\theta, \quad \sin\psi, \quad \frac{k_z}{k}, \quad \frac{B_z}{B}, \tag{39}$$

although we note a relation given by

$$\cos\theta = \frac{k_z B_z + \boldsymbol{k}_{\rm H}\cdot\boldsymbol{B}_{\rm H}}{kB} = \frac{k_z}{k}\frac{B_z}{B} + \frac{k_{\rm H}}{k}\frac{B_{\rm H}}{B}\cos\psi. \tag{40}$$

For a given value of $\cos\theta$, we have

$$\cos\psi = \frac{\cos\theta - (k_z/k)(B_z/B)}{(k_{\rm H}/k)(B_{\rm H}/B)}, \tag{41}$$

and the parameters $k_z/k$ and $B_z/B$ must satisfy an inequality $\cos^2\psi \leq 1$, that is,

$$\left(\frac{k_z}{k}\right)^2 + \left(\frac{B_z}{B}\right)^2 - 2\cos\theta\frac{k_z}{k}\frac{B_z}{B} \leq 1 - \cos^2\theta, \tag{42}$$

which can be rewritten as

$$\frac{x^2}{x_0^2} + \frac{y^2}{y_0^2} \leq 1, \tag{43}$$

where

$$x = \frac{1}{2}\left(\frac{k_z}{k} + \frac{B_z}{B}\right), \quad y = \frac{1}{2}\left(\frac{k_z}{k} - \frac{B_z}{B}\right), \quad x_0^2 = \cos^2\frac{\theta}{2}, \quad y_0^2 = \sin^2\frac{\theta}{2}. \tag{44}$$

In the following discussions, instead of $k_z/k$ and $B_z/B$, it will be convenient to use the parameters $f$ and $\theta_f$ defined by

$$x = x_0 f\cos\theta_f \quad \text{and} \quad y = y_0 f\sin\theta_f \quad \text{with} \quad 0 \leq f \leq 1. \tag{45}$$

Using these parameters we have $k_z/k = f\cos(\theta_f - \theta/2)$ and $B_z/B = f\cos(\theta_f + \theta/2)$, and $p$, $q$, $\bar{N}^2$, $\bar{\Omega}_z$, $(Rk)$, $\cos\theta$, $f$ and $\theta_f$ are the parameters we need to specify.

For the fluid ocean of the model NS05T7, typical values of the parameters $p$ and $\bar{N}^2$ are found to be

$$p \sim 10^{-8}, \quad \bar{N}^2 \sim 10^5, \tag{46}$$

and a typical value of the parameter $q$, depending on $B_0$, is $q \sim 10^{-6}$ for $B_0 \sim 10^7\,{\rm G}$ and $q \sim 1$ for $B_0 \sim 10^{10}\,{\rm G}$. Since $k_{\rm H}/k = \sqrt{1 - f^2\cos(\theta_f - \theta/2)} \ll 1$ for low-frequency modes, we need $f \sim 1$ and $\theta_f \sim \theta/2$. In the following discussions, for simplicity, we assume $f = 0.99$, $\theta_f = \theta/2$ and $g = g_S$. Examples of numerical solutions of the dispersion relation (22) are given in Fig. 7, where $\bar{\omega}$ versus $\bar{\Omega}_z$ is plotted for $\cos\theta = 0.1$ (dotted line), 0.5 (solid line) and 0.9 (dashed line) in the left-hand panel, and $\bar{\omega}$ versus $\bar{\Omega}_z$ for $q = 10^{-8}$ (dotted line), $10^{-6}$ (solid line) and $10^{-4}$ (dashed line) in the right-hand panel. It is interesting to note that the asymmetry due to the term proportional to $A_1$ is too weak to become noticeable in the figure. As shown by the left-hand panel, for a given value of $\cos\theta$, the solution have two branches in this frequency region, and the upper and lower branches, respectively, correspond to gravito-inertial waves, for which $\omega \propto 2|\Omega_z|$ when $|\Omega_z|$ becomes large, and Alfvén waves, for which $\omega \propto a_{\rm A}k\cos\theta$. The minimum frequency in the inertial mode branch and the maximum frequency in the Alfvén mode branch, which occur at $\bar{\Omega}_z \sim 0$, increase as $\cos\theta$ increases. These two branches of modes are

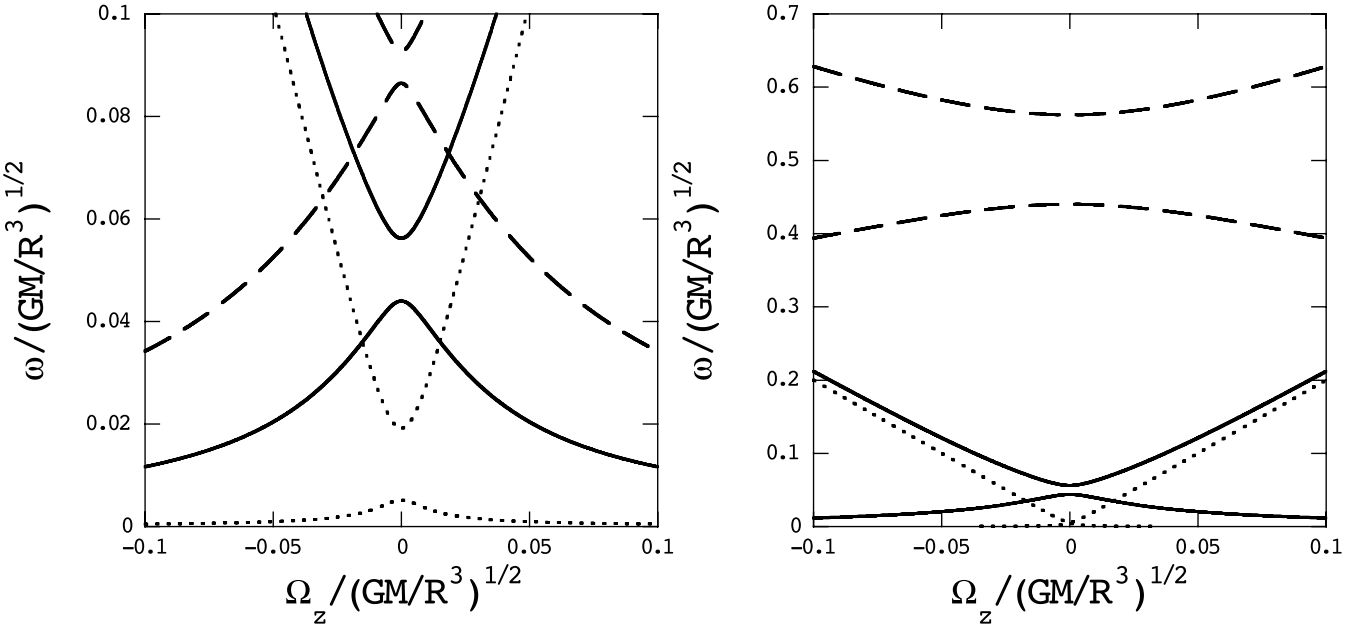


**Figure 7.** Left-hand panel: low-frequency solutions of the dispersion relation (22) plotted as functions of $\bar{\Omega}_z$ for $\cos\theta = 0.1$ (dotted line), 0.5 (solid line) and 0.9 (dashed line), where we have assumed $p = 10^{-8}$, $q = 10^{-6}$, $\bar{N}^2 = 10^5$, $(Rk) = 10^2$, $f = 0.99$, $\theta_f = \theta/2$ and $g = g_S$. Right-hand panel: low-frequency solutions of the dispersion relation (22) plotted as functions of $\bar{\Omega}_z$ for $q = 10^{-4}$ (dashed line), $10^{-6}$ (solid line) and $10^{-8}$ (dotted line), where we have assumed $p = 10^{-8}$, $\cos\theta = 0.5$, $\bar{N}^2 = 10^5$, $(Rk) = 10^2$, $f = 0.99$, $\theta_f = \theta/2$ and $g = g_S$.

reminiscent of the low-frequency waves in the ocean plotted in Fig. 1. We think that the two different mode branches associated with a *mean* angle $\theta$ between $\boldsymbol{B}$ and $\boldsymbol{k}$ appear as a pair of mode branches in Fig. 1 and that the minimum and maximum frequencies at $\Omega/\sqrt{GM/R^3} \sim 0$ in the pair depend on this mean angle, which may vary from one pair to another. As shown by the right-hand panel of Fig. 7, for a given value of $\cos\theta$, the frequency of the Alfvén modes increases as $q$ increases, and the inertial branch tends to the relation given by $\omega = 2|\Omega_z|$ in the limit of $q \to 0$.

## 5 DISCUSSION AND CONCLUSION

Lamb et al. (2009) proposed that the small-amplitude, almost sinusoidal millisecond X-ray pulsation observed in accretion-powered millisecond X-ray pulsars may be well explained by the hotspot model, in which the hotspots are assumed to be located at the magnetic poles, which are nearly aligned with the rotation axis. As discussed by Lamb et al. (2009), even a small drift of the hotspot could produce appreciable changes in pulsation amplitudes of the X-ray pulsation. If this proposition is correct, it is interesting to pursue a possibility of using the millisecond X-ray pulsation to probe the core r modes excited by gravitational wave radiation (Andersson 1998; Friedman & Morsink 1998). In fact, if the core r modes with $|m| \geq 2$ are excited by the emission of gravitational wave, since the $l' = m = 2$ r mode, which is the most strongly destabilized mode among the r modes (e.g. Lockitch & Friedman 1999; Yoshida & Lee 2000a), produces the surface displacement vector $\boldsymbol{\xi}$ whose horizontal and toroidal components at the surface have large amplitudes around the rotation axis as shown in Fig. 6, the hotspot could suffer periodic disturbance from the r mode. Note that the r-mode-induced temperature perturbation, the surface pattern of which may be proportional to $X^r(\theta)\,\mathrm{e}^{\mathrm{i}m\phi}$, might generate X-ray variations, the amplitudes of which should be very small. If we write the oscillation frequency of r modes as

$$\omega/\Omega = \kappa_0 + \kappa_2\bar{\Omega}^2 + O\left(\bar{\Omega}^4\right), \tag{47}$$

the coefficient $\kappa_0$ for the modes is given by

$$\kappa_0 = 2m/\left[l'\left(l'+1\right)\right], \tag{48}$$

and the coefficient $\kappa_2$ may depend on the equation of state and the deviation from the isentropic stratification in the core (e.g. Yoshida & Lee 2000a,b), where $\bar{\Omega} = \Omega/\Omega_0$. Since the neutron star core is nearly isentropic such that $N^2 \sim 0$, we only have to consider the $l' = |m|$ r modes, for which we have $\omega \approx \kappa_0\Omega = 2\Omega/(|m|+1)$, and we obtain the frequency $\omega \approx 2\Omega/3$ for $m = 2$ in the corotating frame of the star and the frequency $\sigma \equiv \omega - m\Omega \approx -4\Omega/3$ in an inertial frame. It may be interesting to point out that if the r mode of $l' = m = 1$ is also excited by some mechanism, this r mode can produce long-period variations in an inertial frame since the inertial frame frequency $\sigma \sim 0$ for this mode. Although no detection of periodicities whose frequency is approximately equal to $4\Omega/3$ has so far been reported, if the periodicities produced by the core r modes of $l' = |m|$ in the X-ray millisecond pulsation are detected, we can use the frequency deviation given by $\Delta\bar{\omega} \equiv \bar{\omega} - \kappa_0\bar{\Omega} \approx \kappa_2\bar{\Omega}^3$ to derive information about the equations of state and the thermal stratification in the core. The detectability of the r-mode pulsation may depend on the thickness of the crust, the property of the fluid ocean, the strength of the magnetic field and so on.

To assess the possibility of detecting periodicities associated with the core r modes, assuming Schwarzschild metric and taking account of the Doppler effects, we have carried out a simple calculation of light curves produced by a circular hotspot, which is assumed to perform periodic drifts, driven by the core $m = 2$ r mode, around a fixed point on the surface of a rapidly rotating neutron star. We find that the fractional rms amplitudes produced by the drift of the hotspot of the angular radius $\sim 20^\circ$ are $\sim 0.01$ for the drift angular radius $\sim 1^\circ$ and the angular distance $\sim 5^\circ$ of the spot centre from the spin axis for the observer inclination angle $30^\circ$, where we assume that the mass of the star is $M = 1.4\,\mathrm{M}_\odot$ and the spin frequency is 600 Hz. The drift angular radius $\sim 1^\circ$ may correspond to the amplitudes of the horizontal displacement vector $|\boldsymbol{\xi}_\mathrm{H}/R| \sim 0.01$ at the surface, which are well in linear regime and could produce detectable contributions to the light curves.

We have calculated non-axisymmetric low-frequency modes of a rotating and magnetized neutron star, where we used a neutron star model composed of a surface fluid ocean, a solid crust and a fluid core. We have assumed that the star is threaded by a dipole magnetic field but the fluid core can be treated as a non-magnetic region. For this model, we found that for a magnetic field of strength $B_0 \sim 10^7$ G, Alfvén waves in the surface ocean come in as low-frequency modes, which largely modify the gravito-inertial modes in the ocean. However, the oscillation frequencies of the modes in the ocean are dependent on $j_\mathrm{max}$, and they do not reach any good convergence even if $j_\mathrm{max}$ is increased to $\sim 20$. At present it is not clear that these ocean modes will converge to discrete modes with real frequencies in the limit of $j_\mathrm{max} \to \infty$. Note that in the absence of a magnetic field the convergence of a mode frequency of a rotating star is mainly affected by the ratio $\nu = 2\Omega/\omega$, and in general we need large $j_\mathrm{max}$ for modes having large $|\nu|$ to get a good convergence. For example, for modes with $l \sim |m|$, we need $j_\mathrm{max} \sim 5$ for $|\nu| \sim 10$, and $j_\mathrm{max} \sim 15$ for $|\nu| \sim 100$. We also found that no r modes confined to the surface ocean can be found in the presence of the weak magnetic field, which may be because of the fact that for $B_0 \gtrsim 10^7$ G the Alfvén frequency in the vertical direction becomes comparable to or greater than the r-mode frequency of an unmagnetized ocean; so the ocean modes are no longer present in their original form. If this is also the case for the accreted envelopes expected in mass-accreting neutron stars in binary systems, we need to reconsider the Rossby wave model for the burst oscillation in LMXBs (Heyl 2004; Lee 2004). On the other hand, the toroidal crust modes and the interfacial modes at the core/crust interface, which show good convergence for $j_\mathrm{max} \gtrsim 10$, are found to be insensitive to magnetic fields of strength $B_0 \lesssim 10^{12}$ G. We also found that the core r modes and inertial modes are not affected by the magnetic field even if their eigenfunctions extend to the surface through the magnetized crustal and envelope regions. We regard the results for $B_0 \lesssim 10^{12}$ G understandable, considering that we have assumed an unmagnetized fluid core with the free-slip jump conditions at the crust/core boundary and that magnetohydrodynamic (MHD) restoring forces are weaker in the crust than the elastic ones by several orders of magnitudes. However, this will not be the case for neutron stars having magnetic fields as strong as $B_0 \sim 10^{15}$ G (e.g. Lee 2008).

For waves propagating in the fluid ocean of a neutron star, Heng & Spitkovsky (2009) carried out a linear analysis of MHD shallow water waves, taking account of the effects of rotation and a magnetic field. Assuming a radial magnetic field at the surface, Heng & Spitkovsky (2009) derived a modified Laplace tidal equation for the angular dependence of the eigenfunctions of the shallow water waves and suggested the existence of two limiting solutions, near-equator solutions and near-pole solutions. Although the configuration of the magnetic field they assumed is not the same as that we use here, their analysis may suggest a possible existence of well-defined ocean modes with real frequencies for a dipole magnetic field.

In this paper, we employed for modal analysis a low-mass neutron star model having a thick solid crust and a cold and thin surface ocean, for which the toroidal crust modes of low radial order and low spherical harmonic degree are well separated from the f and p modes. If we use more massive neutron stars with a hot accreted fluid envelope and a thin solid crust, the frequencies of the crust modes of low radial order and those of the f and p modes may overlap, leading to more complicated frequency spectra. We think it necessary to conduct similar modal analyses for such neutron star models to clarify the properties of the ocean modes in the presence of a magnetic field and to examine the possibility that the small-amplitude millisecond X-ray pulsation can be used as a probe into the core r modes.

## ACKNOWLEDGMENT

I thank Mr T. Numata for calculating light curves produced by a drifting hotspot on a rapidly rotating neutron star.

## REFERENCES

Andersson N., 1998, ApJ, 502, 708
Bastrukov S. I., Chang H.-K., Molodtsova I. V., Wu E.-H., Chen G.-T., Lan S.-H., 2009, Ap&SS, 323, 235
Bildsten L., Cutler C., 1995, ApJ, 449, 800
Cerdá-Durán P., Stergioulas N., Font J. A., 2009, MNRAS, 397, 1607
Colaiuda A., Beyer H., Kokkotas K. D., 2009, MNRAS, 396, 1441
Cumming A., Bildsten L., 2000, ApJ, 544, 453
Cumming A., Morsink S. M., Bildsten L., Friedman J. L., Holz D. E., 2002, ApJ, 564, 343
Duncan R. C., 1998, ApJ, 498, L45
Friedman J. L., Morsink S. M., 1998, ApJ, 502, 714
Glampedakis K., Samuelsson L., Andersson N., 2006, MNRAS, 371, L74
Heng K., Spitkovsky A., 2009, ApJ, 703, 1819
Heyl J. S., 2004, ApJ, 600, 939
Heyl J. S., 2005, MNRAS, 361, 504
Israel G. et al., 2005, ApJ, 628, L53

Lamb F. K., Boutloukos S., Van Wassenhove S., Chamberlain R. T., Lo K. H., Clare A., Yu W., Miller M. C., 2009, ApJ, 706, 417
Lee U., 2004, ApJ, 600, 914
Lee U., 2007, MNRAS, 374, 1015
Lee U., 2008, MNRAS, 385, 2069
Lee U., Saio H., 1990, ApJ, 360, 590
Lee U., Strohmayer T. E., 1996, A&A, 311, 155
Lee U., Strohmayer T. E., 2005, MNRAS, 361, 659
Levin Y., 2006, MNRAS, 367, L35
Levin Y., 2007, MNRAS, 377, 159
Lockitch K. H., Friedman J. L., 1999, ApJ, 521, 764
McDermott P. N., Van Horn H. M., Hansen C. J., 1988, ApJ, 325, 725
Piro A. L., 2005, ApJ, 634, L153
Piro A. L., Bildsten L., 2005, ApJ, 629, 438
Richardson M. B., Van Horn H. M., Ratcliff K. F., Malone R. C., 1982, ApJ, 255, 624
Sotani H., Kokkotas K. D., 2009, MNRAS, 395, 1163
Sotani H., Kokkotas K. D., Stergioulas N., 2008, MNRAS, 385, 5
Strohmayer T. E., Watts A. L., 2005, ApJ, 632, L111
Strohmayer T. E., Watts A. L., 2006, ApJ, 653, 593
Strohmayer T. E., Day C., Smale A. P., Swank J. H., Zhang W., Titarchuk L., Lee U., 1997, ApJ, 486, 355
Unno W., Osaki Y., Ando H., Saio H., Shibahashi H., 1989, Nonradial Oscillations of Stars, 2d edn. University of Tokyo Press, Tokyo
Watts A. L., Strohmayer T. E., 2006, ApJ, 637, L117
Woods P. M., Thompson C., 2006, in Lewin W. H. G., van der Klis M., eds, Compact Stellar X-Ray Sources. Cambridge Univ. Press, Cambridge
Yoshida S., Lee U., 2000a, ApJ, 529, 997
Yoshida S., Lee U., 2000b, ApJS, 129, 353
Yoshida S., Lee U., 2001, ApJ, 546, 1121

## APPENDIX A: OSCILLATION EQUATIONS, JUMP CONDITIONS AND BOUNDARY CONDITIONS

In this appendix, we present the oscillation equations solved for non-axisymmetric ($m \neq 0$) modes of rotating and magnetized neutron stars. As noted in the text (Section 2), we assume a dipole magnetic field whose axis is aligned with the rotation axis. We use Newtonian dynamics, and employ the Cowling approximation, neglecting the Euler perturbation of the gravitational potential. Using the dependent variables defined by

$$(\boldsymbol{y}_1)_j = S_{l_j}, \quad (\boldsymbol{y}_2)_j = \frac{p'_{l_j}}{gr\rho}, \quad (\boldsymbol{y}_3)_j = H_{l_j}, \quad (\boldsymbol{y}_4)_j = iT_{l'_j}, \quad (\boldsymbol{b}^{\rm H})_j = b^{\rm H}_{l'_j}, \quad (\boldsymbol{b}^{\rm T})_j = b^{\rm T}_{l_j}, \quad (\boldsymbol{b}^{\rm S})_j = b^{\rm S}_{l'_j} \tag{A1}$$

and

$$\boldsymbol{y}_5 = \frac{\mathbf{M}_1\boldsymbol{b}^{\rm H} + m\boldsymbol{\Lambda}_0^{-1}{\rm i}\boldsymbol{b}^{\rm T}}{\alpha}, \quad \boldsymbol{y}_6 = \frac{m\boldsymbol{\Lambda}_1^{-1}\boldsymbol{b}^{\rm H} + \mathbf{M}_0{\rm i}\boldsymbol{b}^{\rm T}}{\alpha}, \tag{A2}$$

the oscillation equation for non-axisymmetric modes with $m \neq 0$ for fluid regions threaded by a dipole magnetic field is given by

$$r\frac{{\rm d}\boldsymbol{y}_1}{{\rm d}r} = \left(\frac{V}{\Gamma_1} - 3\right)\boldsymbol{y}_1 - \frac{V}{\Gamma_1}\boldsymbol{y}_2 + \boldsymbol{\Lambda}_0\boldsymbol{y}_3, \tag{A3}$$

$$r\frac{{\rm d}\boldsymbol{y}_2}{{\rm d}r} = \left(rA + c_1\bar{\omega}^2\right)\boldsymbol{y}_1 + (1 - rA - U)\,\boldsymbol{y}_2 - m\nu c_1\bar{\omega}^2\boldsymbol{y}_3 - \nu c_1\bar{\omega}^2\mathbf{C}_0\boldsymbol{y}_4 + \frac{c_1\bar{\omega}^2}{2}\boldsymbol{R}, \tag{A4}$$

$$\mathbf{M}_0 r\frac{{\rm d}\boldsymbol{y}_3}{{\rm d}r} + m\boldsymbol{\Lambda}_1^{-1}r\frac{{\rm d}\boldsymbol{y}_4}{{\rm d}r} = -\frac{1}{2}\left(\frac{V}{\Gamma_1} - 4\right)\mathbf{K}\boldsymbol{y}_1 + \frac{1}{2}\frac{V}{\Gamma_1}\mathbf{K}\boldsymbol{y}_2 + \left(\mathbf{M}_0 - \frac{1}{2}\mathbf{C}_1\right)\boldsymbol{y}_3 + m\boldsymbol{\Lambda}_1^{-1}\boldsymbol{y}_4 - \frac{1}{2}\alpha\frac{\boldsymbol{b}^{\rm H}}{\alpha}, \tag{A5}$$

$$m\boldsymbol{\Lambda}_0^{-1}r\frac{{\rm d}\boldsymbol{y}_3}{{\rm d}r} + \mathbf{M}_1 r\frac{{\rm d}\boldsymbol{y}_4}{{\rm d}r} = \frac{1}{2}\left(\frac{V}{\Gamma_1} - 4\right)m\boldsymbol{\Lambda}_0^{-1}\boldsymbol{y}_1 - \frac{1}{2}\frac{V}{\Gamma_1}m\boldsymbol{\Lambda}_0^{-1}\boldsymbol{y}_2 + m\boldsymbol{\Lambda}_0^{-1}\boldsymbol{y}_3 + \left(\mathbf{M}_1 - \frac{1}{2}\mathbf{C}_0\right)\boldsymbol{y}_4 - \frac{1}{2}\alpha\frac{{\rm i}\boldsymbol{b}^{\rm T}}{\alpha}, \tag{A6}$$

$$r\frac{{\rm d}\boldsymbol{y}_5}{{\rm d}r} = \left(-m\nu\boldsymbol{\Lambda}_0^{-1} + \frac{\mathbf{M}_1\mathbf{C}_0^{\rm T}}{\alpha}\right)\boldsymbol{y}_1 - \frac{\boldsymbol{y}_2}{c_1\bar{\omega}^2} + \left(\mathbf{L}_0 - \frac{2\mathbf{M}_1\boldsymbol{\Lambda}_1\mathbf{M}_0}{\alpha}\right)\boldsymbol{y}_3 - \left(\nu + \frac{2m}{\alpha}\right)\mathbf{M}_1\boldsymbol{y}_4 + \left(2 - \frac{{\rm d}\ln\alpha}{{\rm d}\ln r}\right)\boldsymbol{y}_5 + \frac{m}{2}\frac{{\rm i}\boldsymbol{b}^{\rm T}}{\alpha}, \tag{A7}$$

$$r\frac{{\rm d}\boldsymbol{y}_6}{{\rm d}r} = \left(\nu - \frac{m}{\alpha}\right)\mathbf{K}\boldsymbol{y}_1 - \left(\nu + \frac{2m}{\alpha}\right)\mathbf{M}_0\boldsymbol{y}_3 + \left(\mathbf{L}_1 - \frac{2m^2}{\alpha}\boldsymbol{\Lambda}_1^{-1}\right)\boldsymbol{y}_4 + \left(2 - \frac{{\rm d}\ln\alpha}{{\rm d}\ln r}\right)\boldsymbol{y}_6 - \frac{1}{2}\mathbf{C}_1\frac{{\rm i}\boldsymbol{b}^{\rm T}}{\alpha}, \tag{A8}$$

with

$$\boldsymbol{R} = r\frac{\rm d}{{\rm d}r}\left(\mathbf{C}_0\frac{\boldsymbol{b}^{\rm H}}{\alpha} + m\frac{{\rm i}\boldsymbol{b}^{\rm T}}{\alpha}\right) - \left(2 - \frac{{\rm d}\ln\alpha}{{\rm d}\ln r}\right)\left(\mathbf{C}_0\frac{\boldsymbol{b}^{\rm H}}{\alpha} + m\frac{{\rm i}\boldsymbol{b}^{\rm T}}{\alpha}\right) - \mathbf{C}_0\frac{\boldsymbol{b}^{\rm S}}{\alpha} \tag{A9}$$

and

$$\boldsymbol{b}^{\rm S} = -\boldsymbol{\Lambda}_1\mathbf{K}\boldsymbol{y}_1 - 2\boldsymbol{\Lambda}_1\mathbf{M}_0\boldsymbol{y}_3 - 2m\boldsymbol{y}_4, \tag{A10}$$

where $\nu = 2\Omega/\omega$, $\bar{\omega} = \omega/\sqrt{GM/R^3}$ with $M$ and $R$ being the mass and radius of the star,

$$U = \frac{\mathrm{d}\ln M_r}{\mathrm{d}\ln r}, \quad V = -\frac{\mathrm{d}\ln p}{\mathrm{d}\ln r}, \quad c_1 = \frac{(r/R)^3}{M_r/M}, \quad \alpha = \frac{c_1\bar{\omega}^2 pV}{4p_\mathrm{B}}, \quad p_\mathrm{B} = \frac{B_0^2}{8\pi}, \tag{A11}$$

and $\mathbf{C}_0^\mathrm{T}$ is the transposed matrix of $\mathbf{C}_0$. The non-zero elements of the matrices $\mathbf{M}_0$, $\mathbf{M}_1$, $\mathbf{C}_0$, $\mathbf{C}_1$, $\mathbf{K}$, $\mathbf{\Lambda}_0$ and $\mathbf{\Lambda}_1$ that appear in the oscillation equation given above are defined by

$$(\mathbf{M}_0)_{j,j} = \frac{l_j}{l_j+1}J^m_{l_j+1}, \quad (\mathbf{M}_0)_{j,j+1} = \frac{l_j+3}{l_j+2}J^m_{l_j+2}, \quad (\mathbf{M}_1)_{j,j} = \frac{l_j+2}{l_j+1}J^m_{l_j+1}, \quad (\mathbf{M}_1)_{j+1,j} = \frac{l_j+1}{l_j+2}J^m_{l_j+2}, \tag{A12}$$

$$(\mathbf{C}_0)_{j,j} = -(l_j+2)J^m_{l_j+1}, \quad (\mathbf{C}_0)_{j+1,j} = (l_j+1)J^m_{l_j+2}, \quad (\mathbf{C}_1)_{j,j} = l_j J^m_{l_j+1}, \quad (\mathbf{C}_1)_{j,j+1} = -(l_j+3)J^m_{l_j+2}, \tag{A13}$$

$$(\mathbf{K})_{j,j} = \frac{J^m_{l_j+1}}{l_j+1}, \quad (\mathbf{K})_{j,j+1} = -\frac{J^m_{l_j+2}}{l_j+2}, \quad (\mathbf{\Lambda}_0)_{j,j} = l_j\left(l_j+1\right), \quad (\mathbf{\Lambda}_1)_{j,j} = l'_j\left(l'_j+1\right) \tag{A14}$$

for even modes, and

$$(\mathbf{M}_0)_{j,j} = \frac{l_j+1}{l_j}J^m_{l_j}, \quad (\mathbf{M}_0)_{j+1,j} = \frac{l_j}{l_j+1}J^m_{l_j+1}, \quad (\mathbf{M}_1)_{j,j} = \frac{l_j-1}{l_j}J^m_{l_j}, \quad (\mathbf{M}_1)_{j,j+1} = \frac{l_j+2}{l_j+1}J^m_{l_j+1}, \tag{A15}$$

$$(\mathbf{C}_0)_{j,j} = (l_j-1)J^m_{l_j}, \quad (\mathbf{C}_0)_{j,j+1} = -(l_j+2)J^m_{l_j+1}, \quad (\mathbf{C}_1)_{j,j} = -(l_j+1)J^m_{l_j}, \quad (\mathbf{C}_1)_{j+1,j} = l_j J^m_{l_j+1}, \tag{A16}$$

$$(\mathbf{K})_{j,j} = -\frac{J^m_{l_j}}{l_j}, \quad (\mathbf{K})_{j+1,j} = \frac{J^m_{l_j+1}}{l_j+1}, \quad (\mathbf{\Lambda}_0)_{j,j} = l_j\left(l_j+1\right), \quad (\mathbf{\Lambda}_1)_{j,j} = l'_j\left(l'_j+1\right) \tag{A17}$$

for odd modes, where

$$J^m_l = \sqrt{\frac{l^2-m^2}{4l^2-1}} \tag{A18}$$

for $l \geq |m|$, and $J^m_l = 0$ for $l < |m|$. The matrices $\mathbf{L}_0$ and $\mathbf{L}_1$ are given by

$$\mathbf{L}_0 = \mathbf{1} - m\nu\mathbf{\Lambda}_0^{-1}, \quad \mathbf{L}_1 = \mathbf{1} - m\nu\mathbf{\Lambda}_1^{-1} \tag{A19}$$

with $\mathbf{1}$ being the unit matrix. Note that $l_j = |m| + 2(j-1)$ and $l'_j = l_j + 1$ for even modes, and $l_j = |m| + 2j - 1$ and $l'_j = l_j - 1$ for odd modes.

For a solid region threaded by the dipole magnetic field, on the other hand, we use the dependent variables defined as

$$(z_1)_j = S_{l_j}, \quad (z_2)_j = H_{l_j}, \quad (z_3)_j = iT_{l'_j}, \tag{A20}$$

and

$$z_4 = \left(\Gamma_1 - \frac{2}{3}\alpha_1\right)\left[\frac{1}{r^2}\frac{\mathrm{d}}{\mathrm{d}r}\left(r^3 z_1\right) - \mathbf{\Lambda}_0 z_2\right] + 2\alpha_1\frac{\mathrm{d}}{\mathrm{d}r}\left(rz_1\right) + \frac{2p_\mathrm{B}}{p}\left(\mathbf{C}_0\boldsymbol{b}^\mathrm{H} + m\mathrm{i}\boldsymbol{b}^\mathrm{T}\right) \tag{A21}$$

$$z_5 = \alpha_1\left(r\frac{\mathrm{d}z_2}{\mathrm{d}r} + z_1\right) - \frac{4p_\mathrm{B}}{p}\left(\mathbf{M}_1\boldsymbol{b}^\mathrm{H} + m\mathbf{\Lambda}_0^{-1}\mathrm{i}\boldsymbol{b}^\mathrm{T}\right), \quad z_6 = \alpha_1 r\frac{\mathrm{d}z_3}{\mathrm{d}r} - \frac{4p_\mathrm{B}}{p}\left(m\mathbf{\Lambda}_1^{-1}\boldsymbol{b}^\mathrm{H} + \mathbf{M}_0\mathrm{i}\boldsymbol{b}^\mathrm{T}\right), \tag{A22}$$

where

$$\alpha_1 = \frac{\mu}{p}, \quad \alpha_2 = \Gamma_1 - \frac{2}{3}\alpha_1, \quad \alpha_3 = \Gamma_1 + \frac{4}{3}\alpha_1. \tag{A23}$$

The oscillation equation then becomes

$$r\frac{\mathrm{d}z_1}{\mathrm{d}r} = -\frac{3\Gamma_1}{\alpha_3}z_1 + \frac{\alpha_2}{\alpha_3}\mathbf{\Lambda}_0 z_2 + \frac{1}{\alpha_3}z_4 - \frac{2p_\mathrm{B}}{\alpha_3 p}\left(\mathbf{C}_0\boldsymbol{b}^\mathrm{H} + m\mathrm{i}\boldsymbol{b}^\mathrm{T}\right), \tag{A24}$$

$$\begin{aligned}\mathbf{M}_0 r\frac{\mathrm{d}z_2}{\mathrm{d}r} + m\mathbf{\Lambda}_1^{-1}r\frac{\mathrm{d}z_3}{\mathrm{d}r} &= \frac{1}{2}\left(1 + \frac{3\Gamma_1}{\alpha_3}\right)\mathbf{K}z_1 + \left(\mathbf{M}_0 - \frac{\alpha_2}{2\alpha_3}\mathbf{C}_1\right)z_2 + m\mathbf{\Lambda}_1^{-1}z_3 - \frac{1}{2\alpha_3}\mathbf{K}z_4 \\ &+ \left(\frac{p_\mathrm{B}}{\alpha_3 p}\mathbf{K}\mathbf{C}_0 - \frac{1}{2}\mathbf{1}\right)\boldsymbol{b}^\mathrm{H} + \frac{p_\mathrm{B}}{\alpha_3 p}m\mathbf{K}\mathrm{i}\boldsymbol{b}^\mathrm{T},\end{aligned} \tag{A25}$$

$$\begin{aligned}m\mathbf{\Lambda}_0^{-1}r\frac{\mathrm{d}z_2}{\mathrm{d}r} + \mathbf{M}_1 r\frac{\mathrm{d}z_3}{\mathrm{d}r} &= -\frac{1}{2}\left(1 + \frac{3\Gamma_1}{\alpha_3}\right)m\mathbf{\Lambda}_0^{-1}z_1 + m\left[\mathbf{\Lambda}_0^{-1} + \frac{1}{2}\left(\frac{\alpha_2}{\alpha_3} - 1\right)\mathbf{1}\right]z_2 + \left(\mathbf{M}_1 - \frac{1}{2}\mathbf{C}_0\right)z_3 + \frac{m}{2\alpha_3}\mathbf{\Lambda}_0^{-1}z_4 \\ &- \frac{p_\mathrm{B}}{\alpha_3 p}m\mathbf{\Lambda}_0^{-1}\mathbf{C}_0\boldsymbol{b}^\mathrm{H} - \frac{1}{2}\left(\mathbf{1} + \frac{2p_\mathrm{B}}{\alpha_3 p}m^2\mathbf{\Lambda}_0^{-1}\right)\mathrm{i}\boldsymbol{b}^\mathrm{T},\end{aligned} \tag{A26}$$

$$\begin{aligned}r\frac{\mathrm{d}z_4}{\mathrm{d}r} &= \left[\left(UV - 4V - c_1\bar{\omega}^2 V + \tfrac{12\alpha_1\Gamma_1}{\alpha_3}\right)\mathbf{1} - \tfrac{2p_\mathrm{B}}{p}\mathbf{C}_0\mathbf{\Lambda}_1\mathbf{K}\right]z_1 + \left[mc_1\bar{\omega}^2 V\nu\mathbf{1} + \left(V - 2\alpha_1 - \tfrac{4\alpha_1\alpha_2}{\alpha_3}\right)\mathbf{\Lambda}_0 - \tfrac{4p_\mathrm{B}}{p}\mathbf{C}_0\mathbf{\Lambda}_1\mathbf{M}_0\right]z_2 \\ &+ \left(c_1\bar{\omega}^2 V\nu - \frac{4p_\mathrm{B}}{p}m\right)\mathbf{C}_0 z_3 + \left(V - \frac{4\alpha_1}{\alpha_3}\right)z_4 + \mathbf{\Lambda}_0 z_5 + \frac{4p_\mathrm{B}}{p}\left[\mathbf{\Lambda}_0\mathbf{M}_1 - 2\left(1 - \frac{\alpha_1}{\alpha_3}\right)\mathbf{C}_0\right]\boldsymbol{b}^\mathrm{H} - \frac{4p_\mathrm{B}}{p}\left(1 - \frac{2\alpha_1}{\alpha_3}\right)m\mathrm{i}\boldsymbol{b}^\mathrm{T},\end{aligned} \tag{A27}$$

$$r\frac{\mathrm{d}\boldsymbol{z}_5}{\mathrm{d}r} = \left[\left(V - \tfrac{6\alpha_1\Gamma_1}{\alpha_3}\right)\mathbf{1} + mc_1\bar{\omega}^2 V\nu\boldsymbol{\Lambda}_0^{-1} + \tfrac{4p_\mathrm{B}}{p}\mathbf{M}_1\boldsymbol{\Lambda}_1\mathbf{K}\right]\boldsymbol{z}_1 + \left[-c_1\bar{\omega}^2 V\mathbf{L}_0 + \tfrac{8p_\mathrm{B}}{p}\mathbf{M}_1\boldsymbol{\Lambda}_1\mathbf{M}_0 - 2\alpha_1\mathbf{1} + 2\alpha_1\left(1 + \tfrac{\alpha_2}{\alpha_3}\right)\boldsymbol{\Lambda}_0\right]\boldsymbol{z}_2$$
$$+ \left(c_1\bar{\omega}^2 V\nu + \frac{8mp_\mathrm{B}}{p}\right)\mathbf{M}_1\boldsymbol{z}_3 - \left(1 - \frac{2\alpha_1}{\alpha_3}\right)\boldsymbol{z}_4 + (V-3)\,\boldsymbol{z}_5 + \frac{4p_\mathrm{B}}{p}\left[\mathbf{M}_1 + \left(\frac{1}{2} - \frac{\alpha_1}{\alpha_3}\right)\mathbf{C}_0\right]\boldsymbol{b}^\mathrm{H} + \frac{4p_\mathrm{B}}{p}m\left(\boldsymbol{\Lambda}_0^{-1} - \frac{\alpha_1}{\alpha_3}\mathbf{1}\right)\mathrm{i}\boldsymbol{b}^\mathrm{T}, \quad \text{(A28)}$$

$$r\frac{\mathrm{d}\boldsymbol{z}_6}{\mathrm{d}r} = \left(-c_1\bar{\omega}^2 V\nu + \tfrac{4p_\mathrm{B}}{p}m\right)\mathbf{K}\boldsymbol{z}_1 + \left(c_1\bar{\omega}^2 V\nu + \tfrac{8p_\mathrm{B}}{p}m\right)\mathbf{M}_0\boldsymbol{z}_2 + \left[-c_1\bar{\omega}^2 V\mathbf{L}_1 + \tfrac{8p_\mathrm{B}}{p}m^2\boldsymbol{\Lambda}_1^{-1} - 2\alpha_1\left(\mathbf{1} - \tfrac{1}{2}\boldsymbol{\Lambda}_1\right)\right]\boldsymbol{z}_3$$
$$+ (V-3)\,\boldsymbol{z}_6 + \frac{4p_\mathrm{B}}{p}m\boldsymbol{\Lambda}_1^{-1}\boldsymbol{b}^\mathrm{H} + \frac{4p_\mathrm{B}}{p}\left(\mathbf{M}_0 + \frac{1}{2}\mathbf{C}_1\right)\mathrm{i}\boldsymbol{b}^\mathrm{T}. \quad \text{(A29)}$$

We derive one set of the jump conditions imposed at the interface between the solid crust and the fluid ocean by assuming the continuity condition of the displacement vector at the interface (see e.g. Lee 2007):

$$[\boldsymbol{\xi}\,(r_i)]_-^+ = 0, \quad \text{(A30)}$$

where $[F\,(r_i)]_-^+ \equiv \lim_{\epsilon\to 0}\,[F(r_i+\epsilon) - F(r_i-\epsilon)]$. The other set of the jump conditions is derived from the continuity condition of the $rr$, $r\theta$ and $r\phi$ components of the perturbed traction at the interface:

$$\left[\delta\tau_{rj}\,(r_i)\right]_-^+ = 0, \quad \text{(A31)}$$

where $\delta\tau_{ij}$ denotes the $ij$ component of the perturbed traction, and the detail expression of $\delta\tau_{ij}$ is given in Lee (2007). As for the jump conditions at the interface between the solid crust and the fluid core, which is assumed non-magnetic, we use the continuity of the radial component of the displacement vector and of the $rr$, $r\theta$ and $r\phi$ components of the perturbed traction at the interface.

The surface boundary conditions for non-axisymmetric modes are given by

$$\delta p/p = 0, \quad \mathrm{i}\boldsymbol{b}^\mathrm{T} = 0, \quad \boldsymbol{b}^\mathrm{S} + L^+\boldsymbol{b}^\mathrm{H} = 0, \quad \text{(A32)}$$

where $\delta p$ denotes the Lagrangian perturbation of the pressure, and $L^+ = \delta_{ij}(l_j' + 1)$ (Lee 2007). As for the inner boundary conditions at stellar centre, we require that the functions $r\boldsymbol{y}_1$ and $r\boldsymbol{y}_2$ are regular at the centre.

This paper has been typeset from a TEX/LATEX file prepared by the author.